ARTICLE IN PRESS

Theoretical Population Biology xxx (xxxx) xxx

Contents lists available at ScienceDirect

Theoretical Population Biology

journal homepage: www.elsevier.com/locate/tpb

Coevolution fails to maintain genetic variation in a host–parasite model with constant finite population size

Ailene MacPherson [a,*], Matthew J. Keeling [b], Sarah P. Otto [a]

[a] Department of Zoology and Biodiversity Research Centre, University of British Columbia, Vancouver, Canada
[b] Zeeman Institute of Systems Biology and Infectious Disease Research (SBIDER), University of Warwick, Coventry, United Kingdom

ARTICLE INFO

Article history:
Received 15 April 2020
Available online xxxx

Keywords:
Coevolution
Genetic variation
Matching-alleles
Negative frequency-dependent selection

ABSTRACT

Coevolutionary negative frequency-dependent selection has been hypothesized to maintain genetic variation in host and parasites. Despite the extensive literature pertaining to host–parasite coevolution, the temporal dynamics of genetic variation have not been examined in a matching-alleles model (MAM) with a finite population size relative to the expectation under neutral genetic drift alone. The dynamics of the MA coevolution in an infinite population, in fact, suggests that genetic variation in these coevolving populations behaves neutrally. By comparing host heterozygosity to the expectation in a single-species model of neutral genetic drift we find that while this is also largely true in finite populations two additional phenomena arise. First, reciprocal natural selection acting on stochastic perturbations in host and pathogen allele frequencies results in a slight increase or decrease in genetic variation depending on the parameter conditions. Second, following the fixation of an allele in the parasite, selection in the MAM becomes directional, which then rapidly erodes genetic variation in the host. Hence, rather than maintain it, we find that, on average, matching-alleles coevolution depletes genetic variation.

© 2020 Elsevier Inc. All rights reserved.

1. Introduction

There is a rich history of evolutionary theory exploring the conditions under which genetic variation is maintained or depleted in finite populations. The loss of genetic variation through drift is exacerbated, for example, by fluctuations in population size (Crow, 1970, Eq. 7.6.3.34), but variation is maintained through balancing selection in the form of overdominance (Crow, 1970, Eq. 8.6.4) or negative frequency-dependent selection (Takahata and Nei, 1990). First suggested by Haldane (1949), one process that is often posited to maintain genetic variation is coevolution between hosts and their parasites. Coevolution, it is argued, should favour pathogens that are best at infecting the most common host genotype. This in turn should favour the spread of rare host genotypes, a form of negative frequency-dependent selection (NFDS) believed to maintain genetic variation (Clarke, 1979).

Following Haldane's initial hypotheses, balancing selection as a result of coevolution and/or overdominance was suggested as a mechanism behind the extraordinary genetic diversity found at mammalian Major Histocompatibility Complex (MHC) loci (Bodmer, 1972). These same arguments have been used recently to explain the diversity of anti-microbial peptides in *Drosophila* (Unckless et al., 2016; Chapman et al., 2019). MHC loci, and other immune defence genes, are notable not only for their high levels of heterozygosity ($>$ 200 alleles across three loci Klein and Figueroa, 1986; Zimmer and Emlen, 2013) but also for the long-term trans-specific persistence of these polymorphisms (Lawlor et al., 1988; Klein, 1987). Using a coalescent approach in a single species Takahata and Nei (1990) found that heterozygote advantage and NFDS are both capable of generating the observed levels of polymorphism. Importantly, however, the model of NFDS they used was not explicitly coevolutionary but rather explored frequency-dependent selection within a single species. Despite the long-standing interest in coevolution as a mechanism maintaining genetic variation, it remains unclear whether NFDS between species in a coevolutionary model is able to maintain more genetic variation in a finite population than expected under neutral processes alone and hence contribute to the excess genetic diversity observed at immune defence genes.

As exemplified by Takahata and Nei (1990), much of the literature on the maintenance of genetic variation alludes to yet blurs the distinction between single-species and coevolutionary NFDS (for example see Tellier et al., 2014; Otto and Michalakis, 1998; Zhao and Waxman, 2016; Llaurens et al., 2017; Ejsmond and Radwan, 2015; Rabajante et al., 2016). By the definition of

* Corresponding author.
E-mail address: amacp@zoology.ubc.ca (A. MacPherson).

https://doi.org/10.1016/j.tpb.2020.12.001
0040-5809/© 2020 Elsevier Inc. All rights reserved.

Please cite this article as: A. MacPherson, M.J. Keeling and S.P. Otto, Coevolution fails to maintain genetic variation in a host–parasite model with constant finite population size. Theoretical Population Biology (2020), https://doi.org/10.1016/j.tpb.2020.12.001.

NFDS in a single-species model (also called direct-NFDS, Brown and Tellier, 2011), the fitness of an allele increases as its frequency declines, which can favour the spread of rare alleles and the maintenance of genetic variation. By contrast, coevolutionary NFDS (also called indirect-NFDS), the sort that commonly arises with host–parasite coevolution, favours alleles of the focal species that correspond to ones that are rare in the interacting species. As noted by Brown and Tellier for the gene-for-gene model (2011), we show that coevolutionary NFDS in the matching-alleles model often has little if any impact on the maintenance of genetic variation relative to neutral drift.

Hints that coevolutionary NFDS does not maintain genetic variation can be found throughout the theoretical literature on matching-alleles models. Simulating coevolution in a population where genetic variation is repeatedly introduced through migration or mutation, Frank (1991, 1993) found that the dynamics were dominated by the fixation and loss of genetic variants. He attributed this effect to the repeated population bottlenecks that occur from coevolutionary driven fluctuations in population size, but it was unclear whether this same behaviour would arise in a population of constant size. Similarly, although not explicitly discussed, many individual-based models of coevolution include mutation in either one (Agrawal and Lively, 2002) or both species (Lively, 1999; Borghans et al., 2004; Ejsmond and Radwan, 2015) in order to maintain variation and hence coevolution over the long term. Modelling coevolution in an infinite population, M'Gonigle et al. (2009) found that genetic variation is not maintained at equilibrium except when mutation is very frequent. This is echoed in simulations in finite populations, where in the absence of mutation/migration, allele fixation in either the host or pathogen is very rapid (Gokhale et al., 2013; Schenk et al., 2018). In addition to including mutation, there are several theoretical indications that, rather than being driven by NFDS, the emergent effects of coevolution are dependent on the existence of heterozygote advantage in diploids. For example, M'Gonigle and Otto (2011) showed that the evolution of parasitism depends, not solely on NFDS, but on whether the interaction induces heterozygote advantage, on average. Similarly, Nuismer and Otto (2004) showed that whether there is, on average, heterozygote advantage is the key determinant of how ploidy levels evolve in both hosts and parasites.

Despite this long and extensive history of verbal and theoretical models, it is unclear whether coevolutionary NFDS can indeed maintain genetic variation at a single locus and hence contribute to extensive diversity observed at immune defence loci. Here we compare the maintenance of genetic variation in finite coevolving populations relative to that expected under neutral drift. Previous studies of the MAM in finite populations have focused instead on the relative advantage of host versus parasite (Veller et al., 2017), the number of alleles maintained by mutation (Borghans et al., 2004; Xue and Goldenfeld, 2017), and the time to fixation/loss of alleles in either host or parasite with and without ecological feedbacks (Gokhale et al., 2013; Schenk et al., 2020). We aim to understand the effect of host–parasite interactions on the maintenance of genetic variation, relative to the neutral expectation, by examining a simple single-locus model of coevolution with constant population sizes, where some analytical progress is possible. Metaphorically, we seek to understand when the Red Queen, defined here as coevolutionary maintenance of polymorphism in both hosts and pathogens, collapses because of the loss of polymorphism in one species or the other.

2. Theoretical background

There are two classic models of coevolution involving a single locus major-effect genes in each species, the gene-for-gene model (GFGM), which was motivated by the genetic architecture of flax-rust interactions (Flor, 1956), and the matching-alleles model (MAM), a form of host–parasite specificity that may arise from lock and key molecular interactions (Dybdahl et al., 2014).

When and how genetic variation is maintained in the GFGM is relatively well understood. In the GFGM, hosts carry either a "susceptible" or "resistant" allele. Susceptible hosts can be infected by both "virulent" and "avirulent" parasite genotypes, whereas resistant hosts can only be infected by the virulent parasite genotype. (Brown and Tellier, 2011) identify three factors promoting the existence of a balanced polymorphism in models with GFG interactions and hence the maintenance of genetic variation in finite populations. First, genetic factors (e.g., dominance interactions that result in overdominance in diploids) can result in stable polymorphisms when costs to host resistance and parasite virulence are introduced (Ye et al., 2003; Sasaki, 2000). Second, polymorphisms can be favoured by asynchrony between host and pathogen allele frequency dynamics. This includes both temporal asynchrony resulting, for example, from seed dormancy or perenniality (Tellier and Brown, 2009) and spatial asynchrony arising from population structure. Finally, stable polymorphisms can arise in the GFGM via eco-evolutionary or epidemiological-evolutionary feedbacks (Brown and Tellier, 2011; Ashby et al., 2019).

The maintenance of genetic variation in the MAM is much less well understood. MA coevolution is often formulated, and simulated, as an interaction between a host and pathogen with discrete non-overlapping generations (Nuismer, 2017). In each generation hosts are exposed to a single parasite. If host and parasite carry the same, "matching", allele at the coevolutionary locus then infection occurs with probability X whereas interactions between "mis-matching" host and parasite genotypes occur at a reduced rate Y. Successful infection decreases host fitness by α_H and increases parasite fitness by α_P. The host and pathogen population sizes are often assumed to remain constant in these models such that hosts and pathogens reproduce proportionally to their fitness creating a subsequent generation of the same size.

In the deterministic (infinite population size) limit, the resulting recursion equations for the MAM are characterized by an unstable cyclic equilibrium at an allele frequency of 1/2 in both the host (p_H) and the parasite (p_P), as shown in Fig. 1A (M'Gonigle et al., 2009; Segar and Hamilton, 1988). To examine the effect of coevolution on the maintenance of genetic variation we consider the evolutionary dynamics of host heterozygosity, measured here as the "expected heterozygosity", the probability two alleles drawn at random from the haploid population are different $H = 2p_H(1 - p_H)$. The resulting dynamics of host heterozygosity is shown in Fig. 1B. Starting from a small perturbation near the polymorphic equilibrium, heterozygosity in the host population begins near its maximum of 0.5 and declines, on average, as the allele frequencies cycle outward. Thus, while coevolutionary NFDS generates allele frequency cycles in the short term, these cycles grow in amplitude over time and are not expected to maintain genetic variation in the long term except in the presence of very high mutation rates (M'Gonigle et al., 2009). Indeed, simulating the discrete-time MAM in a finite population, we confirm that host heterozygosity in this model declines faster than expected under neutral genetic drift (see supplementary *Mathematica* notebook). Supplementary materials are available on Dryad at doi:10.5061/dryad.m37pvmd0z.

In contrast to the unstable Red Queen cycles generated in discrete time, analogous continuous-time models create neutrally stable allele frequency cycles (Woolhouse et al., 2002). Perturbations from the polymorphic equilibrium in these models lead to allele frequency cycles of constant amplitude, often referred to as a "dynamic polymorphism" (Hamilton, 1993). This dynamic

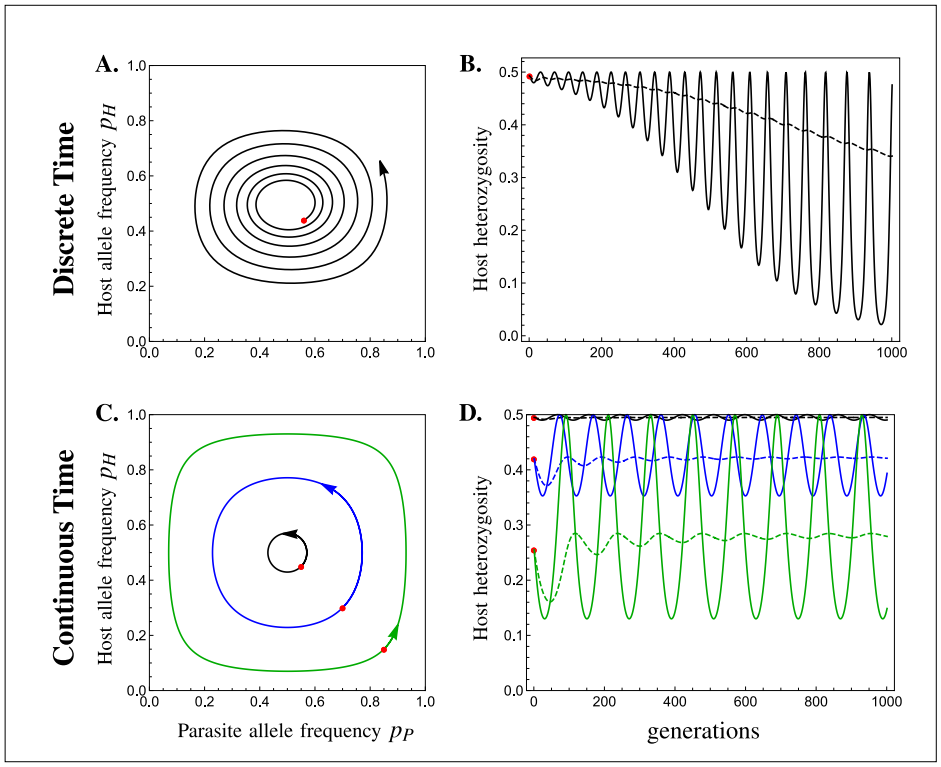

Fig. 1. Deterministic dynamics of matching-alleles coevolution. Panel A: Phase-plane diagram of the unstable allele frequency cycles of the discrete-time matching-alleles model given by system (A.11) starting from a small initial perturbation (red point) from the polymorphic equilibrium. Parameters: $X = 0.8, Y = 0.4, \alpha = 0.4, t_{max} = 1000$. Initial conditions: Black $p_H(0) = 0.54$, $p_P(0) = 0.47$. Panel B: Solid line gives corresponding temporal dynamics of host heterozygosity whereas dashed line gives host heterozygosity averaged over time. Panel C: Phase plane of neutrally stable allele frequency cycles arising in the continuous-time MAM given by system (3) starting form three different initial conditions shown by the red points. Parameters: $X = 0.8, Y = 0.4, \kappa = 100, \delta = 1, \alpha = 0.2, \gamma = 1, t_{max} = 1000$. Initial conditions: Black $p_H(0) = 0.55$, $p_P(0) = 0.45$, Blue $p_H(0) = 0.7$, $p_P(0) = 0.3$, Green $p_H(0) = 0.85$, $p_P(0) = 0.15$. Panel D: Host heterozygosity at each given time point (solid) and averaged over time (dashed). (For interpretation of the references to colour in this figure legend, the reader is referred to the web version of this article.)

polymorphism gives rise to corresponding cycles in heterozygosity also of constant amplitude (Fig. 1C). This neutral stability indicates that, when averaged over the cycle, genetic variation remains constant in an infinite population, much like the behaviour of a neutral locus in a single-species model. We thus hypothesize that drift in a finite population may have similar effects in the coevolutionary model as in the neutral single-species model. Our aim here is therefore to develop an appropriate continuous-time MAM of coevolution in a finite population of constant size that, like the standard continuous-time MAM, does not lead to an inherent decline in heterozygosity in the deterministic limit. This formulation of the MAM allows us to quantify the loss of heterozygosity with drift in direct comparison to a standard model of neutral genetic drift within a single-species.

All the models discussed thus far make the traditional assumption that both host and parasite densities are infinite and controlled by factors independent of the host–parasite interaction. This is the case, for example, when host and parasite population sizes are fixed by a hard carrying capacity that is very large. The numbers of hosts and parasites may, however, vary dramatically in response to coevolution (Papkou et al., 2016). In addition parasites that are transmitted directly between hosts may be subject to epidemiological dynamics. Both ecological (Ashby et al., 2019) and epidemiological (MacPherson and Otto, 2018) feedback can stabilize allele frequency dynamics. Ecological feedback has also been shown to affect the time until allele fixation in either the host or parasite (Gokhale et al., 2013; Schenk et al., 2020). Our goal in this work, however, is to focus solely on the effects that arise from coevolutionary NFDS. Specifically, we examine the stochastic nature of coevolutionary dynamics, allowing us to quantify rates of loss of genetic variation. To do so, we focus on the simplest case of strict external control of population size in both hosts and parasites without ecological or epidemiological feedback.

3. The model

We use a continuous-time birth–death model to describe the coevolutionary dynamics between a host and a free-living pathogen, as depicted in Fig. 2. To keep the total host and pathogen population sizes constant at the same fixed value κ, we use a Moran model design with coupled birth–death events. Extension of the model to unequal host and pathogen population sizes is straightforward and the results do not differ qualitatively from those presented here (MacPherson et al., 2020). Both host and pathogen are haploid, with coevolution depending on a single biallelic locus in each species. We represent the number of hosts and pathogens of each type by H_i and P_j where $i \in \{1, 2\}$ and $j \in \{1, 2\}$. Hosts of type i come into contact with pathogens of type j at a density-independent rate $\frac{H_i P_j}{\kappa}$. In keeping with the MAM, upon contact the pathogen successfully infects the host with probability $\beta_{i,j}$. If the host and pathogen carry "matching" alleles ($i = j$) then $\beta_{i,j} = X$, whereas "mis-matching" infection occurs with a reduced probability $\beta_{i,j} = Y < X$ for $i \neq j$. If infection occurs, hosts die instantaneously with probability α. The resulting rate of fatal infection of host type i from pathogen type j is $\frac{\alpha \beta_{i,j} H_i P_j}{\kappa}$. Fatal infections result in four coupled events (1) the death of the infected host of type i, (2) birth of a random host, (3) birth of the infecting pathogen of type j representing

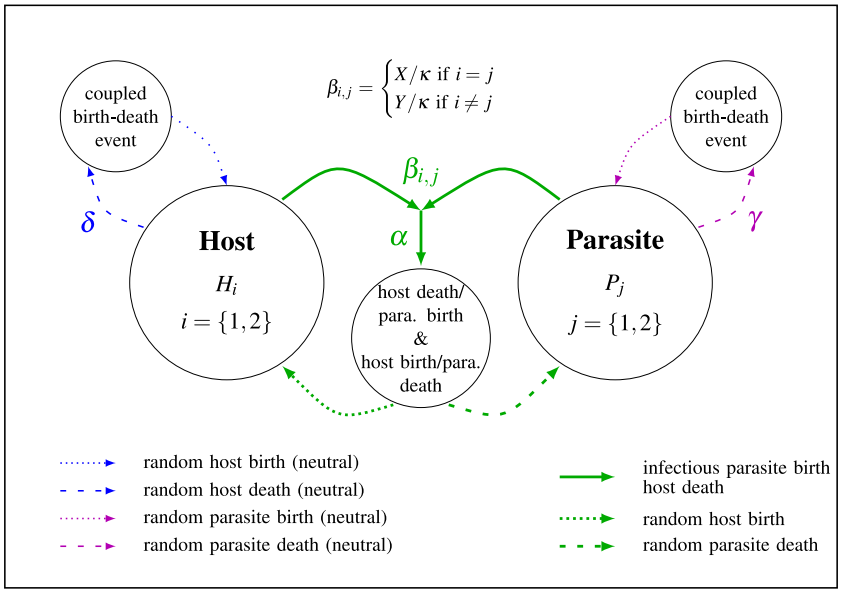

Fig. 2. Schematic of the Moran MAM. Coevolution consisting of three different types of coupled birth–death events. Infection (green/thick), natural host death (blue/thin), and free-living pathogen death (purple/standard). Solid lines denote events that occur at a rate that depends on the genotype whereas dashed arrows represent birth and death of random individuals irrespective of their genotype. (For interpretation of the references to colour in this figure legend, the reader is referred to the web version of this article.)

the release of infectious particles, and (4) death of a random pathogen. Non-fatal infections do not lead to the birth or death of either the host or pathogen, effectively assuming that the pathogen mounts a very limited infection and returns to the free-living pathogen population. In addition to these four events associated with infections, natural host death–birth and free-living pathogen death–birth occur at per-capita rates δ and γ, respectively. Both events are non-selective consisting of the death and birth of random host and pathogen genotypes.

As stated above, our primary aim is to compare the maintenance of genetic variation in a finite coevolving population to that expected under neutral genetic drift alone. Focusing on genetic variation in the host, for a population of finite size κ, the expected decline in host heterozygosity from neutral genetic drift in the haploid Moran model is given by:

$$H_{neut}(t) = H_0 e^{\frac{-2t}{\kappa}}, \tag{1}$$

where H_0 is the initial host heterozygosity and time, t, is measured in units of host generations (Moran, 1958; Wakeley, 2016). In this continuous-time coevolutionary model we define one host generation as the expected time to the death of κ hosts, $1/D$ (see Appendix A.1), where

$$\frac{1}{D} = \frac{\sum_{i,j} \beta_{i,j} \alpha H_i P_j + \sum_i \delta H_i}{\kappa}. \tag{2}$$

As D depends on both the host and pathogen allele frequencies, its value changes over time as the species evolve. We confirm that this is indeed the appropriate scaling of absolute time into host generations by comparing equation (1) to neutral individual-based simulations described below. One consequence of rescaling time in terms of host, as opposed to parasite, generations is that the rate of genetic drift in the parasite will exceed that of the host if $\gamma > \delta$, increasing the likelihood the parasite will become fixed for one type before the host does. As the generation time of the host and parasite are both a function of infection rate, however, this difference in the rate of drift is small.

3.1. Deterministic dynamics

In the limit as the total host and pathogen population size goes to infinity ($\kappa \to \infty$) the dynamics of the host and pathogen allele frequencies $p_H = H_1/\kappa$ (hence: $1 - p_H = H_2/\kappa$) and $p_P = P_1/\kappa$ (hence: $1 - p_P = P_2/\kappa$) are given by the following system of differential equations (see Appendix A.1):

$$\begin{aligned} \frac{dp_H(t)}{dt} &= \frac{(X-Y)\alpha\,(1-2p_P(t))\,p_H(t)\,(1-p_H(t))}{X\alpha + \delta - (X-Y)\alpha\,(p_P(t) + p_H(t)\,(1-2p_P(t)))} \\ \frac{dp_P(t)}{dt} &= -\frac{(X-Y)\alpha\,(1-2p_H(t))\,p_P(t)\,(1-p_P(t))}{X\alpha + \delta - (X-Y)\alpha\,(p_P(t) + p_H(t)\,(1-2p_P(t)))}, \end{aligned} \tag{3}$$

where time t is in units of host generations as in Eq. (1).

As shown in Fig. 1, the behaviour of this Moran MAM in the deterministic limit is identical to that of the traditional continuous-time MAM (Woolhouse et al., 2002). Specifically, there are five equilibria of system (3). Four are unstable equilibria characterized by the fixation of one host and one pathogen genotype. The final polymorphic equilibria at $\hat{p}_H = \hat{p}_P = \frac{1}{2}$ is neutrally stable with purely imaginary leading eigenvalues, generating neutral-limit cycles in allele frequencies (see Fig. 1C).

As discussed previously, genetic variation neither increases nor decreases over time in the deterministic continuous-time MAM (see Fig. 1D). While the neutral stability of the MAM is well known, the consequences on heterozygosity are under-appreciated. Contrary to the proposed effect of coevolution and NFDS on genetic variation (Haldane, 1949; Clarke, 1979), neutrally stable allele frequency cycles neither deplete nor restore genetic variation. Rather, in an infinite population, coevolution has no net effect on genetic variation, averaged across a cycle. To see if this behaviour holds in finite coevolving populations, we begin by describing an analytical approach to compare the dynamics of genetic variation in a finite population to those expected under neutral genetic drift. Because this analytical approach only applies while the cycles are small we couple this approach with an individual-based simulation describing the loss of genetic variation more generally.

3.2. Ensemble moment dynamics

To model the dynamics of genetic variation in a finite population we express the model depicted in Fig. 2 as a continuous-time Markov chain. The complexity of the model limits the available analytical approaches. One approach we can use, however, is

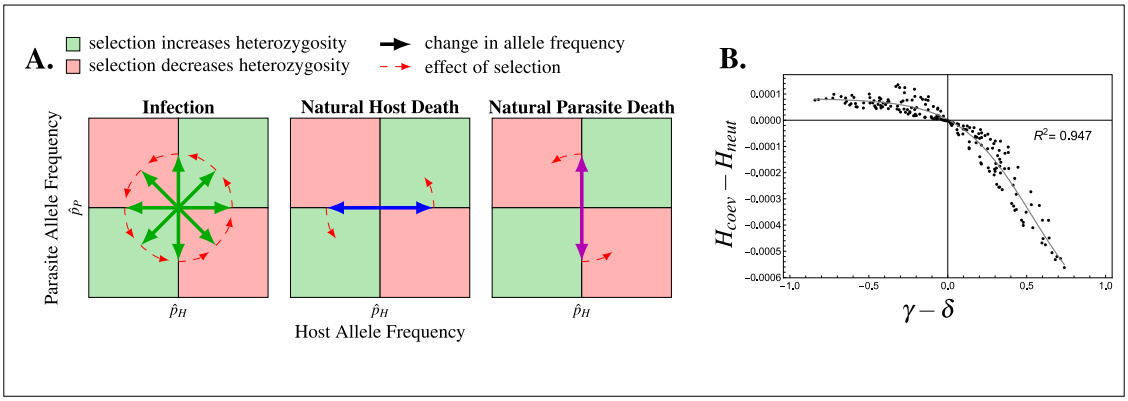

Fig. 3. The effect of early perturbations. Panel A: The effects of the three processes on host heterozygosity shown schematically, infection (green see Fig. 2), natural host death (blue), and natural pathogen death (purple) on host and pathogen allele frequency and the resulting effect of selection (red arrows) on host heterozygosity. Panel B: $H_{coev} - H_{neut}$ as given by the ensemble moment approximation as a function of the relative host and pathogen death rates. Points give the deviation at time $t = 50$ host generations for 200 randomly drawn combinations of γ and δ, where $0.1 < \gamma < 1$, $0.1 < \delta < 1$, and $X = 0.9, Y = 0.7, \alpha = 0.2, \kappa = 10^5$. R^2 describes the non-linear model fit to the sigmoidal function $y = a + \frac{b}{1+e^{-c(x-d)}}$. (For interpretation of the references to colour in this figure legend, the reader is referred to the web version of this article.)

the ensemble moment approximation, the derivation of which is given in the Appendix. The result is an approximation for the expected host heterozygosity which we will call $H_{coev}(t)$. As with the neutral expectation in Eq. (1), this is the expectation of host heterozygosity over all realizations of the stochastic process, the approximation of which is given by a Taylor series assuming the system is near the deterministic equilibrium ($H_0 \approx 1/2$) and the population size large.

$$H_{coev}(t) \approx H_0 \left(1 - \frac{2t}{\kappa}\right) + \mathcal{O}(\epsilon^3) \tag{4}$$

where ϵ is the deviation of the stochastic process from the deterministic equilibrium and $\epsilon = 1/\kappa$. Once again t is measured in units of host generations. To this order, the ensemble moment dynamics are identical to that of the neutral expectation given by (1). Hence, as expected from the deterministic dynamics, host heterozygosity in the MAM declines as expected under neutral genetic drift. Although analytically unwieldy, numerical evaluation of H_{coev} to third order reveals slight deviations between the ensemble moment dynamics and the neutral expectation that are also observed in the individual-based simulations presented in the following section. Specifically, H_{coev} exceeds the neutral expectation when the free-living pathogen death rate γ is less than the death rate of the host δ (negative values of $\gamma - \delta$ in Fig. 3B) and falls below the neutral expectation when $\gamma - \delta > 0$.

The mechanism behind these lower-order deviations is shown schematically in Fig. 3A. If we start, for example, at the equilibrium host and pathogen allele frequencies ($\hat{p}_H = 0.5$, $\hat{p}_P = 0.5$), infection, natural host death–birth, and free-living pathogen death–birth events perturb the allele frequencies. Selection then acts on those perturbations to produce small counter-clock wise allele frequency cycles. Although over the long term these allele frequency cycles have no net effect on heterozygosity, they do have an effect over the short term. For example, if only the host allele frequency is perturbed by a random host birth event then during the first quarter cycle natural selection will increase host heterozygosity, because the parasite that matches the host that, by chance, became more common, will spread in turn reducing the more common host genotype. In contrast, if only the pathogen allele frequency is perturbed, selection will decrease host heterozygosity by preferentially killing off the host that matches the parasite allele that increased by drift.

The effect of these early quarter cycle responses to selection would average out if perturbations were distributed uniformly about the equilibrium. However, natural host death affects only the host allele frequency whereas free-living pathogen death only affects the pathogen allele frequency. Hence the relative rates of these two events determine whether these early responses to selection transiently increases or decreases heterozygosity. Specifically, relatively high rates of natural host death and low rates of free-living pathogen death ($\gamma - \delta < 0$) lead to an increase in host heterozygosity relative to the neutral expectation (see Fig. 3B).

3.3. Individual-based simulations

Using a Gillespie algorithm we simulated host–parasite coevolution in a finite population. In short, the waiting time for the next event is drawn at random from an exponential distribution with a rate parameter given by the sum of the rates to all possible next events (Table A.1). Which of these next events actually occur is then determined randomly by a multinomial assignment with $n = 1$. This is repeated and time is measured in units of generations as determined by the death of κ hosts. Individual based simulations were implemented in C++ (available at doi:10.5061/dryad.m37pvmd0z) For each of one-hundred randomly drawn parameter sets, we simulated coevolution for seven different populations sizes ranging on a log scale from $\kappa = 10^2$ to $\kappa = 10^{3.5} = 3162$. The relative infection rates of matching and mis-matching genotypes were drawn such that $0 \leq Y < X \leq 1$. We restricted the probability of dying from infection, α, to lie between 0 and 1/2 as much stronger selection causes the rapid loss of alleles, limiting the amount of coevolution. Host and pathogen free-living natural death rates δ and γ were both drawn between 0.1 and 1. For each of the 700 parameter sets, we simulated 1000 replicate populations for $t_{max} = 500$ host generations. All replicate populations begin at the internal equilibrium with $p_H = p_P = 0.5$.

In tandem with each coevolutionary replicate population we simulated an analogous "neutral population" to check that it behaved correctly according to the neutral expectation given in Eq. (1). In these simulations, the exact same series of host and pathogen birth–death events occurred as in the coevolutionary simulations, except that the individual who was born or died due to infection was drawn at random hence capturing neutral genetic drift in both host and pathogen. As shown in Fig. 4A, the mean heterozygosity of these neutral simulations in grey is identical to the analytical neutral expectation given by Eq. (1), confirming that this is the appropriate neutral expectation for the two-species model.

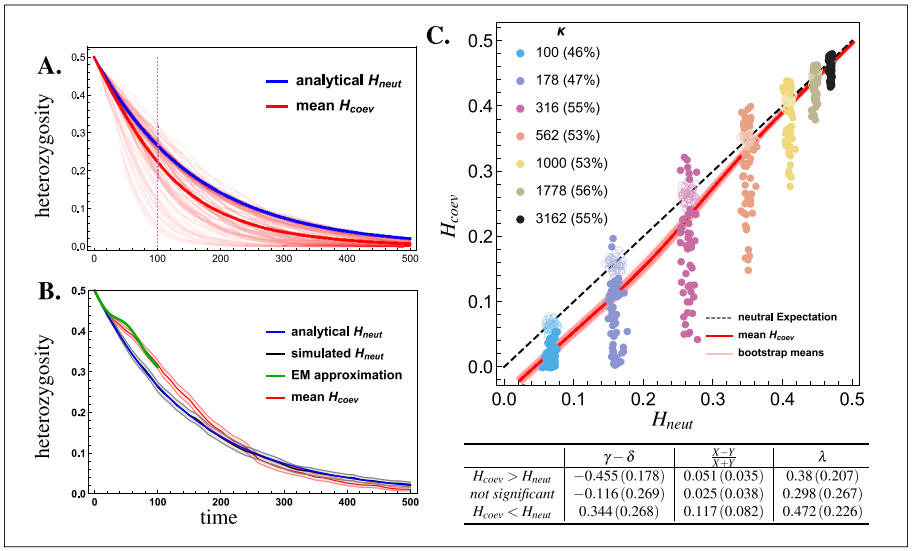

	$\gamma-\delta$	$\frac{X-Y}{X+Y}$	λ
$H_{coev} > H_{neut}$	−0.455 (0.178)	0.051 (0.035)	0.38 (0.207)
not significant	−0.116 (0.269)	0.025 (0.038)	0.298 (0.267)
$H_{coev} < H_{neut}$	0.344 (0.268)	0.117 (0.082)	0.472 (0.226)

Fig. 4. Individual-based simulations. Panel A: Light red lines give mean heterozygosity across replicate populations for each of the 100 parameter sets (given $\kappa = 316$). Dark red line gives mean heterozygosity across parameter sets. Blue line gives analytical neutral expectation. Vertical dashed line corresponds to the time point shown in panel C at $t = 100$. Panel B: An example of simulations for one of the parameter sets that maintains more heterozygosity than the neutral expectation in panel A ($X = 0.39$, $Y = 0.13$, $\alpha = 0.38$, $\delta = 0.99$, $\gamma = 0.24$, $\kappa = 316$). Red curve (red shaded area) gives mean heterozygosity across the 1000 replicate populations each starting at the polymorphic equilibrium (red shaded area gives 95% confidence interval). Black curve (grey shaded area) gives mean (95% CI) heterozygosity in neutral model. Blue curve gives the analytical neutral expectation from Eq. (1). Green curve gives ensemble moment approximation. Panel C: Mean heterozygosity in coevolutionary simulations H_{coev} for each parameter set compared to the corresponding simulated neutral model H_{neut}. Black dashed line gives the neutral expectation. Thick red curve gives LOESS smoothed mean fit whereas light red curves give smoothed mean fit to 100 bootstrap samples. Table gives the mean (standard deviation) of the relative turnover rates $\gamma - \delta$, leading eigenvalue λ, and strength of reciprocal natural selection $\frac{X-Y}{X+Y}$ for points falling significantly above, not significantly different from, and significantly below the neutral expectation. (For interpretation of the references to colour in this figure legend, the reader is referred to the web version of this article.)

Fig. 4 summarizes the results of the individual-based simulations. Panel A illustrates the mean heterozygosity for each set of parameters using $\kappa = 316$. Panel B illustrates one particular parameter set where more heterozygosity is maintained than expected under the neutral model because of a high natural death rate in the host. As illustrated in panel B, the ensemble moment approximation given in Eq. (4) accurately predicts the dynamics of host heterozygosity early on. Hence, as predicted by this approximation, early on host heterozygosity deviates either slightly above or below the neutral expectation depending on the relative turnover rates in the host versus the parasite. In panel C, we show the heterozygosity observed in hosts versus the neutral expectation at generation $t = 100$, where each dot represents the mean heterozygosity among the 1000 replicate simulations for a given parameter set. Whether points fall above or below the neutral expectation is well predicted by $\gamma - \delta$. Given in the table in Fig. 4, $\gamma - \delta$ is negative for points significantly above the neutral expectation and positive for those that are significantly below.

While initial departures are due mainly to the effect of perturbations (Fig. 3), heterozygosity over longer time frames is dominated by a second phenomenon. Shown in Fig. 5A, following allele fixation/loss in the pathogen, natural selection in the matching-allele model becomes directional (red trajectories), favouring whichever host allele is better able to resist the remaining pathogen type. This directional selection rapidly erodes genetic variation within the host, typically resulting in the fixation of the mis-matching host allele and rapidly decreasing host heterozygosity (see the Fig. 5B). The effect of directional selection following allele fixation in the pathogen is strong enough that even for parameter sets with host heterozygosity initially above the neutral expectation (Fig. 4B), heterozygosity eventually falls below the neutral expectation.

One consequence of re-scaling time in terms of host rather than parasite generations is that the parasite will experience slightly more (less) genetic drift than the host and hence more (less) rapid fixation of genetic variation whenever $\gamma > \delta$ ($\gamma < \delta$). The effect of the relative rates of drift in the host and parasite due to these differences in generation times is small and overwhelmed by the effect of selection on early perturbations described above. Other factors that might be expected to influence host heterozygosity include the strength of reciprocal natural selection, as measured by $(X - Y)/(X + Y)$, and the period of the Red Queen allele frequency cycles, as measured by the leading eigenvalue ($\lambda = i\frac{(X-Y)\alpha}{(X+Y)\alpha+2\delta}$). In contrast to the relative turnover rates in the two species (shown in Fig. 3), the mean value of these parameters does not differ among parameter sets with heterozygosity greater than, less than, or not significantly different from the neutral expectation, see table in Fig. 4.

In summary then, as predicted by the neutral stability of the deterministic model, host heterozygosity in the MAM behaves by-and-large neutrally. At generation 100, 52% of parameter conditions shown in Fig. 4C do not statistically differ from the neutral expectation and the average deviation of H_{coev} (red curve) from the neutral expectation (black dashed diagonal) is small. Of the remainder, the majority of parameter sets result in less heterozygosity than neutral (overall, 10% are significantly above and 38% are significantly below the neutral line). The variability in $H_{coev} - H_{neut}$ can be explained mechanistically by both the effect of natural selection on perturbations from the equilibrium (Fig. 3 and the probability of directional selection following pathogen fixation (Fig. 5). These results are consistent across host population sizes, κ, which as we expect by Eq. (1) only changes the rate of genetic drift.

4. Discussion

Contrary to theories that posit that host–parasite coevolution and the associated negative frequency-dependent selection (NFDS) should maintain genetic variation (Haldane, 1949; Clarke, 1979; Takahata and Nei, 1990), we use stochastic methods, both

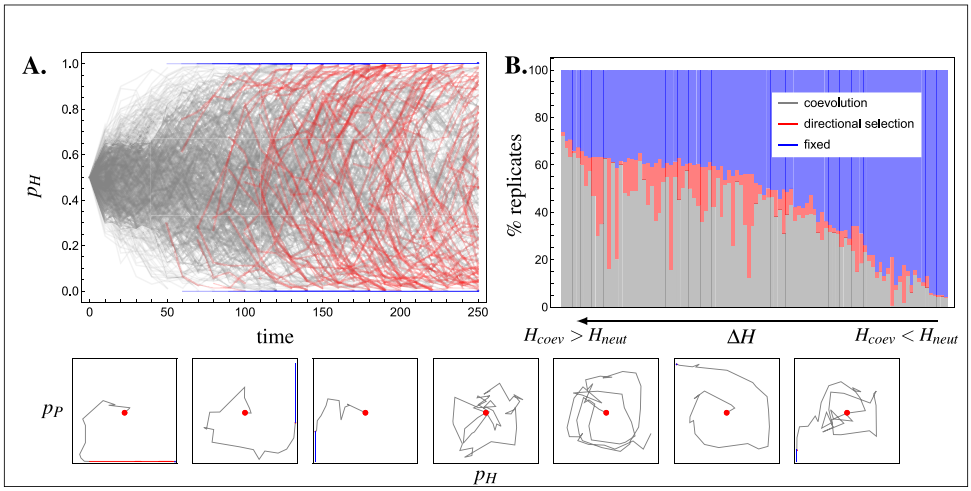

Fig. 5. Effect of directional selection on the long term dynamics of host genetic variation. Panel A. Host allele frequency trajectories for the 1000 replicate populations for a single parameter set ($X = 0.15$, $Y = 0.1$, $\alpha = 0.34$, $\delta = \gamma = 0.21$, and $\kappa = 562$). Trajectory coloured grey while both host and pathogen are polymorphic (ongoing coevolution), red if only the host remains polymorphic (directional selection), and blue if one allele is fixed in the host. Panel B. Each bar corresponds to one parameter set and gives the frequency of replicates at $t = 250$ exhibiting ongoing coevolution, directional selection, or host allele fixation. Bars are ordered with respect to decreasing average H_{coev} across replicate demes. Bottom Row: randomly chosen trajectories shown in the allele frequency phase plane. Trajectories begin at the internal equilibrium (red point) and are coloured as in panel A. (For interpretation of the references to colour in this figure legend, the reader is referred to the web version of this article.)

describing ensemble moments and conducting individual-based simulations, to show that genetic variation is often lost faster than in the neutral model. Although these results are consistent with stability analyses of the corresponding deterministic models, such stability analyses only apply near the equilibrium with equal allele frequencies. In contrast to single-species NFDS, we thus find that coevolutionary NFDS does not generally maintain genetic variation. Specifically, the neutrality of the cycles ensures that, for any given host allele frequency, selection is equally likely to favour or disfavour the allele, depending on the point in the cycle. While the largely neutral effect of matching-alleles coevolution is recovered in our models of finite-population size, we find that stochasticity introduces two new effects. First is the effect of the initial response to selection following perturbations in allele frequency from the deterministic equilibrium, which may on average either maintain or deplete heterozygosity depending on the relative death rates of the host and pathogen. The second non-neutral effect is that of directional selection following the fixation of one of the pathogen alleles, after which host genetic variation rapidly erodes in the host.

The contrasting effects of coevolutionary NFDS and single-species NFDS have been pointed out previously by Brown and Tellier (2011) in the context of the gene-for-gene coevolutionary model. Nevertheless, the distinction between these two processes and in particular their differing effects on the maintenance of genetic variation remains under-appreciated. Our finding that the MAM does not inherently maintain genetic variation contrasts with and clarifies the findings of previous computational models of the maintenance of genetic variation at MHC loci (Ejsmond and Radwan, 2015; Borghans et al., 2004). Simulating matching-alleles coevolution at multiple loci in the presence of rapid host mutation, both Ejsmond and Radwan (2015) and Borghans et al. (2004) find a weak signal of increased fitness of rare host alleles. Our results clarify, however, that this is not in fact a true signal of negative frequency-dependent selection. Rather this is a result of the fact that novel, and hence rare, host alleles may be favoured transiently if there does not yet exist genetic variation at the corresponding pathogen locus. In contrast, long term changes in host allele frequencies are not associated with corresponding changes in fitness as would be required under NFDS (see Borghans et al., 2004 Fig 4A).

Here we have focused on coevolution in a single population. Coevolution is however inherently a spatial process. Previous theoretical models suggest that spatial structure in combination with variability in the strength and nature of host–parasite coevolution across space may promote local adaptation (Gandon et al., 1996; Nuismer, 2006). Our results illustrate, however, that this is an emergent effect of spatial structure and gene flow, not solely the result of coevolution within each individual deme. Whether these spatial models maintain more genetic variation than expected under neutral drift remains a valuable topic for future work.

In the main text we have focused on host–parasite coevolution in a continuous-time model as opposed to a model of coevolution in discrete time (see Eq. (A.11)). This is because, as explored in the background section, the continuous-time model is more likely to maintain genetic variation based on the behaviour of the deterministic dynamics. We confirmed that heterozygosity is lost faster in discrete-time host–parasite models by extending our analysis to a Wright–Fisher model where the entire host and pathogen population is replaced each generation (see Appendix). As illustrated in Fig. A.1, heterozygosity measured relative to the neutral expectation was significantly lower in the discrete-time MAM than in the continuous-time model (i.e., the mean value of $\left(H^{WF}_{coev} - H^{WF}_{neut}\right)$ was significantly less then the mean of $\left(H^{Moran}_{coev} - H^{Moran}_{neut}\right)$). The stability of the deterministic model is therefore a good but not perfect, predictor of the dynamics of host heterozygosity in a finite population and could be used to generate hypotheses about the maintenance of genetic variation in more complex models of host–parasite coevolution.

Given that genetic variation typically erodes at similar or faster rates in MAM than in a single species neutral model, we conclude that coevolutionary NFDS is an insufficient explanation for the long-term persistence of polymorphisms found at immunodefence loci (Lawlor et al., 1988; McConnell et al., 1988; Takahata and Nei, 1990). The models presented here, however, make several implicit assumptions that may influence the maintenance of genetic variation at single loci and their contribution to this broader multi-locus diversity. In particular, we assume that mutations are absent and that the population size remains constant. Mutations can replenish lost genetic variability, allowing Red Queen cycles to continue, or they can introduce new parasite types followed by new hosts that resist them in an ever increasing

arms race. Although constant population size is a classic assumption in coevolutionary theory, coevolution is known to have drastic effects on population sizes of both host and pathogen in natural systems (Papkou et al., 2016). Indeed inclusion of explicit population size dynamics in the MAM results in fluctuations in host and pathogen population size (Nuismer, 2017; Frank, 1993). While these changes in population size are expected to have little to no effect on the allele frequency dynamics, they are expected to have important consequences on the maintenance of genetic variation (Crow, 1970). We also assume that the host and parasite generations are synchronized. The extensive literature on the deterministic stability of the polymorphic equilibrium has suggested that temporal asynchrony between the host and parasite, arising for example through seed dormancy, can stabilize polymorphisms and maintain variation (Brown and Tellier, 2011; Tellier and Brown, 2009). Developing an analogous MAM, we find that here too including a temporal delay in the ability of one species to respond to the other (here by including seed dormancy) has a stabilizing effect and can help maintain variation (see the Appendix).

The abundance of genetic diversity at human MHC loci may also be the result of coevolution between hosts and pathogens that are transmitted directly from one host to another and hence subject to epidemiological dynamics. Our previous work showed that these epidemiological dynamics stabilize Red Queen allele frequency cycles resulting in a stable polymorphic equilibrium (MacPherson and Otto, 2018). In contrast to the instability of the discrete-time MAM and the neutral stability of the continuous-time MAM, the stabilizing effects of these epidemiological dynamics are expected to maintain genetic variation. In a parallel paper, we have found that adding ecological or epidemiological feedback does not greatly help maintain genetic variation. Indeed, population size fluctuations can make parasite populations more likely to lose an allele, leading to directional selection and rapid depletion of variation in the host (MacPherson et al., 2020). Thus, our main conclusion is that negative frequency dependent selection that acts via another species is generally not a strong mechanism for preserving genetic variation.

Declaration of competing interest

The authors declare that they have no known competing financial interests or personal relationships that could have appeared to influence the work reported in this paper.

Acknowledgements

We thank Matt Pennell, Jonathan Davies, Jeff Joy, Dan Coombs, Aurélien Tellier, and two anonymous reviewers for their many helpful suggestions that improved this manuscript. This project was supported by the Godfrey-Hewitt Mobility Award, the AAUW dissertation fellowship, and a fellowship from the University of British Columbia, Canada to A.M. as well as a Natural Sciences and Engineering Research Council of Canada grant to S.P.O. (RGPIN-2016-03711).

Appendix

A.1. Derivation of Eq. (3)

Here we derive the ODEs given by Eq. (3). Shown by the arrows in Fig. 2, host and pathogen allele frequencies change as a result of the 24 different possible events and summarized in Table A.1. To facilitate comparison to the neutral expectation of genetic drift given by Eq. (1) we must rescale absolute time in terms of host generations. If the total rate at which hosts die is given by d, then one host generation, which we define as the expected time until κ deaths is $D = \frac{\kappa}{d}$. In the MAM time in generations, t, then is given by $t = \frac{\tau}{D}$ where τ is time in absolute units and D is given by:

$$D(\tau) = \frac{\kappa}{\sum_{i,j} \beta_{i,j}\alpha H_i(\tau)P_j(\tau) + \sum_i \delta H_i(\tau)} \tag{A.1}$$

Noting that host allele frequency is $p_H = \frac{H_1}{\kappa}$ and pathogen allele frequency is $p_P = \frac{H_2}{\kappa}$ the differential equations for each are given by:

$$\begin{aligned} \frac{dp_H}{dt} &= \frac{1}{\kappa}\frac{dH_1}{d\tau}\frac{d\tau}{dt} = \frac{D}{\kappa}\sum_e f_e(\tau)\Delta_e H_1 \\ \frac{dp_H}{dt} &= \frac{1}{\kappa}\frac{dH_1}{d\tau}\frac{d\tau}{dt} = \frac{Dd}{\kappa}\sum_e f_e(\tau)\Delta_e P_1 \end{aligned} \tag{A.2}$$

where $f_e(\tau)$ is the rate at which event e occurs and $\Delta_e H_1$ ($\Delta_e P_1$) is the change in the number of hosts (parasites) of type 1 due to that event as listed in Table A.1. Substituting in the values and simplifying gives system (3) in the main text (see supplementary *Mathematica* file).

A.2. The ensemble moment approximation

A.2.1. General approach

We consider the general stochastic process in Z^{+n}. Specifically, for the MAM model presented here $n = 2$, one dimension for the number of hosts of type 1 and pathogens of type 1, respectively. Let $\vec{z}(t)$ denote the state of the process at time t, for our case $\vec{z} = \{H_1, P_1\}$. We begin by transforming the variables into their deviation from the deterministic equilibrium. Specifically if $\hat{z}_i$ is the value of variable i at equilibrium, then the transformed variables are given by $\vec{x} = \vec{z} - \hat{\vec{z}}$. In addition, we only consider the case where the initial condition of the stochastic processes is the deterministic equilibrium, $\vec{x} = \vec{0}$. This transformation in variables will then allow us to easily express the moments of the stochastic process in terms of Taylor series around the deterministic equilibrium. In terms of the transformed variables, the stochastic process is described by m distinct events that occur at rates $f_e(\vec{x})$ where $e = \{1, 2, \ldots, m\}$. Finally, we denote the ensemble average, the average across all sample paths, by $\langle * \rangle$.

The aim of the ensemble moment approximation is to derive a system of ODEs giving the change in the moments of the stochastic process. Beginning with the first moment (mean) we have:

$$\begin{aligned} \frac{d\langle x_i\rangle}{dt} &= \langle \sum_{e=1}^{m} (\text{event rates})\,(\text{change in } x_i \text{ from event})\rangle \\ &= \langle \sum_{e=1}^{m} f_e\left(\vec{x}\right)\left(\left(x_i + \Delta_{e,i}\right) - x_i\right)\rangle \end{aligned} \tag{A.3}$$

where $\Delta_{e,i}$ is the change in x_i from event e (Keeling, 2000). To take the ensemble average of the sum we express the argument as a polynomial by approximating it with a Taylor series around the deterministic equilibrium assuming $x_i \,\forall\, i$ is small. Eq. (A.3) is then approximated as:

$$\frac{d\langle x_i\rangle}{dt} \approx \langle \sum_{j}^{m} a_j x_j + \sum_{j,k}^{m,m} b_{j,k} x_j x_k + \sum_{j,k,l}^{m,m,m} c_{j,k,l} x_j x_k x_l + \cdots \rangle \tag{A.4}$$

where a_j, $b_{j,k}$, and $c_{j,k,l}$ are constants, which are themselves functions of the deterministic equilibrium $\hat{\vec{z}}$. Rearranging we have:

$$\frac{d\langle x_i\rangle}{dt} \approx \sum_{j}^{m} a_j \langle x_j\rangle + \sum_{j,k}^{m,m} b_{j,k}\langle x_j x_k\rangle + \sum_{j,k,l}^{m,m,m} c_{j,k,l}\langle x_j x_k x_l\rangle + \cdots \tag{A.5}$$

Table A.1
MAM events. The 24 possible events as given by arrows in Fig. 2. The effect of event e on the number of hosts (parasites) of type 1 is given by $\Delta_e H_1$ ($\Delta_e P_1$). The rate of event in units of host generations as used in the EM approximation is given by $f_e(t) = f_e(\tau)D$.

Description	$\{i, j, k, l\}$	Rate $f_e(\tau)$	e	$\Delta_e H_1$	$\Delta_e P_1$
Random death of host i and birth of host k	{1, NA, 1, NA}	$\delta H_i(\tau)\frac{H_k(\tau)}{\kappa}$	$2(k-1)+i$	0	0
	{1, NA, 2, NA}			−1	0
	{2, NA, 1, NA}			1	0
	{2, NA, 2, NA}			0	0
Random death of parasite j and birth of parasite l	{NA, 1, NA, 1}	$\gamma P_j(\tau)\frac{P_l(\tau)}{\kappa}$	$2(l-1)+j+4$	0	0
	{NA, 1, NA, 2}			0	−1
	{NA, 2, NA, 1}			0	1
	{NA, 2, NA, 2}			0	0
Infection of host i by parasite j: death of host i, birth of host k. Birth of parasite j, death of parasite l.	{1, 1, 1, 1}	$\alpha\beta_{i,j}H_i(\tau)P_j(\tau)\times\frac{H_k(\tau)}{\kappa}\frac{P_l(\tau)}{\kappa}$	$i+4(j-1)+2(k-1)+l$	0	0
	{1, 1, 1, 2}			0	−1
	{1, 1, 2, 1}			−1	0
	{1, 1, 2, 2}			−1	−1
	{1, 2, 1, 1}			0	1
	{1, 2, 1, 2}			0	0
	{1, 2, 2, 1}			−1	1
	{1, 2, 2, 2}			−1	0
	{2, 1, 1, 1}			1	0
	{2, 1, 1, 2}			1	−1
	{2, 1, 2, 1}			0	0
	{2, 1, 2, 2}			0	−1
	{2, 2, 1, 1}			1	1
	{2, 2, 1, 2}			1	0
	{2, 2, 2, 1}			0	1
	{2, 2, 2, 2}			0	0

The result is an expression for the change in the first moment as a linear function of the first, second, third, and higher moments.

We use the same technique to derive the second moment ODEs:

$$\begin{aligned}\frac{d\langle x_i x_j\rangle}{dt} &= \langle \sum_e f_e(\vec{x})\left(\left(x_i+\Delta_{e,i}\right)\left(x_j+\Delta_{e,j}\right)-x_i x_j\right)\rangle \\ &= \langle \sum_e f_e(\vec{x})\left(x_i\Delta_{e,j}+x_j\Delta_{e,i}+\Delta_{e,i}\Delta_{e,j}\right)\rangle\end{aligned} \tag{A.6}$$

Approximating the right-hand argument as a sum once again by a Taylor series expansion we have:

$$\frac{d\langle x_i x_j\rangle}{dt} \approx \sum_j^m A_j\langle x_j\rangle + \sum_{j,k}^{m,m} B_{j,k}\langle x_j x_k\rangle + \sum_{j,k,l}^{m,m,m} C_{j,k,l}\langle x_j x_k x_l\rangle + \cdots \tag{A.7}$$

Similarly for the third moments:

$$\frac{d\langle x_i x_j x_k\rangle}{dt} \approx \sum_j^m \mathcal{A}_j\langle x_j\rangle + \sum_{j,k}^{m,m} \mathcal{B}_{j,k}\langle x_j x_k\rangle + \sum_{j,k,l}^{m,m,m} \mathcal{C}_{j,k,l}\langle x_j x_k x_l\rangle + \cdots \tag{A.8}$$

where A, B, C, $\mathcal{A}$, $\mathcal{B}$, and $\mathcal{C}$ are all constants that depend on the deterministic equilibrium.

A.2.2. Dynamics of host heterozygosity

We are interested in the dynamics of host heterozygosity and calculate the ensemble moment approximation for the dynamics of heterozygosity, H_{coev}:

$$\begin{aligned}\frac{dH_{coev}}{dt} &= \frac{d}{dt}\left(E[2p_H(1-p_H)]\right) = 2\frac{d}{dt}E[p_H - p_H^2] \\ &= 2\left(\frac{d}{dt}\frac{\langle H_1\rangle}{\kappa} - \frac{d}{dt}\frac{\langle H_1^2\rangle}{\kappa^2}\right)\end{aligned} \tag{A.9}$$

The dynamics of heterozygosity thus depends directly on that of the first two moments. If we substitute in Eqs. (A.5) and (A.7) and assume that population size is large $\kappa = 1/\epsilon$, then approximated to $\mathcal{O}(\epsilon^2)$ the dynamics of host heterozygosity simplify to Eq. (4) given in the main text.

A.3. Maintenance of genetic variation in discrete time

A.3.1. Wright–Fisher model specification

Here we model host–parasite coevolution in discrete time with non-overlapping generations with a Wright–Fisher model with a constant host and pathogen population size κ. In each generation, hosts come into contact with a single random pathogen. If host and pathogen have the same genotype i, the probability of successful infection is given by $\beta_{i,i} = X$, whereas hosts of type i are infected by pathogens of mis-matching genotype j, with probability $\beta_{i,j} = Y < X$. In the absence of infections hosts and pathogens have a fitness 1, whereas infection decreases host fitness by a factor α_H and increases pathogen fitness by α_P such that the expected fitness of host genotype i and pathogen genotype j are given by:

$$\begin{aligned}W_H(i,t) &= 1-\alpha_H\sum_j \beta_{i,j}\frac{P_j}{\kappa} \\ W_P(j,t) &= 1+\alpha_P\sum_i \beta_{i,j}\frac{H_i}{\kappa}\end{aligned} \tag{A.10}$$

A.3.2. Deterministic dynamics

As we do for the continuous-time model, we begin by developing an understanding of the effect of coevolution on genetic variation in a finite population by analysing the dynamics of heterozygosity in the limit as the population size goes to infinity. In this deterministic case the coevolutionary dynamics are given by the following difference equations:

$$\begin{aligned}p_H(t+1) &= p_H + \frac{\alpha_H p_H(1-p_H)(1-2p_P)(X-Y)}{\alpha_H(p_H(1-2p_P)+p_P)(X-Y)-\alpha_H X+1} \\ p_P(t+1) &= p_P - \frac{\alpha_P p_P(1-p_P)(1-2p_H)(X-Y)}{-\alpha_P(p_H(1-2p_P)+p_P)(X-Y)+\alpha_P X+1}\end{aligned} \tag{A.11}$$

There are five equilibria of this model, four of these specify the fixation/loss of one host and one pathogen type, and a fifth internal equilibrium occurs at $p_H = p_P = 1/2$. Unlike the continuous time model explored in the main text this internal equilibrium is unstable and cyclic. The dynamics of the allele

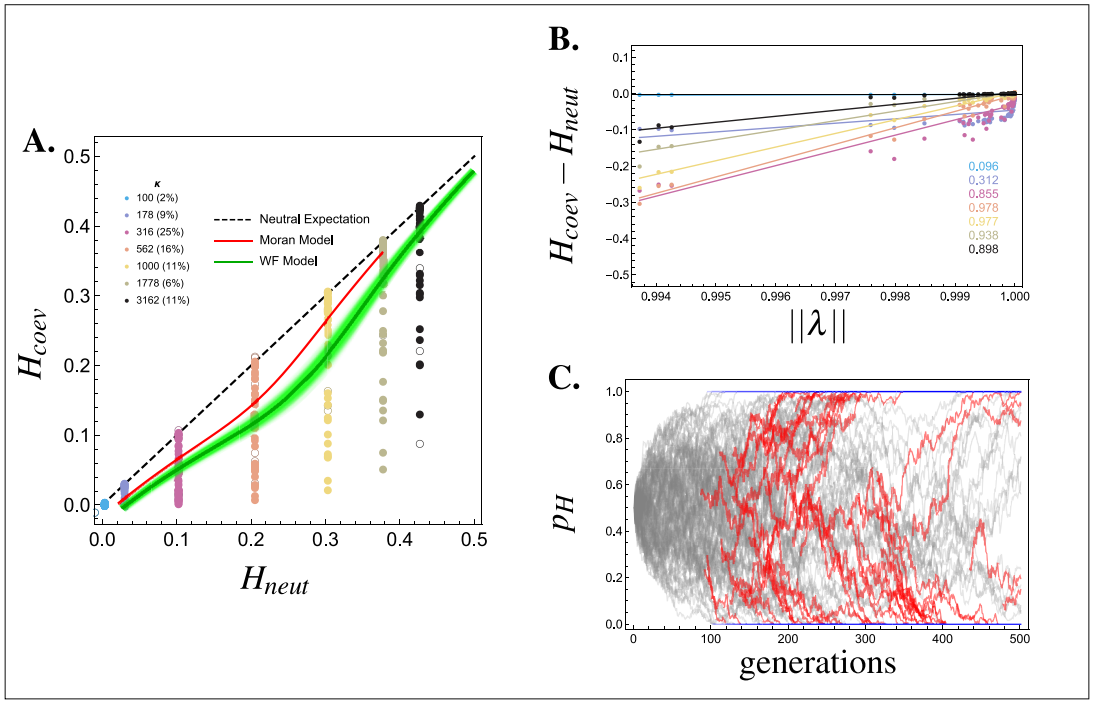

Fig. A.1. Comparison between Wright–Fisher (discrete-time) and Moran (continuous-time) models. Panel A: Mean heterozygosity in a coevolving population versus the neutral expectation for the Wright–Fisher model (green) at time $t = 500$ generations versus. Light green curves give smoothed fits to 1000 bootstrap samples in the WF model. Points depict heterozygosity for each of the 420 (60×7) parameter conditions simulated for the WF model averaged over the 1000 replicate populations. Red curve gives the mean heterozygosity across parameter combinations for the Moran model with values limited to $H_{neut} < 0.375$ to avoid extrapolation beyond the simulated values at this time. Panel B: Deviation in heterozygosity from the neutral expectation in the WF as a function of the magnitude of the leading eigenvalue. R^2 values are given for the linear model fits. Panel C: Example allele frequency dynamics in the WF model. Allele frequency trajectories are coloured grey when there is ongoing coevolution, red when there is directional selection, and blue when the host population is fixed. Parameters: $X = 0.27, Y = 0.07, \alpha = 0.24, \kappa = 10^{2.5} = 316$. (For interpretation of the references to colour in this figure legend, the reader is referred to the web version of this article.)

frequency and heterozygosity are shown in Fig. 1 panels A and B, respectively. The rate at which the amplitude of the cycles grow is given by the magnitude of the leading eigenvalue, which is given by $\|\lambda\|$, a result consistent with those of M'Gonigle et al. (2009).

$$\|\lambda\| = \sqrt{1 + \frac{\alpha_H \alpha_P (X - Y)^2}{(2 - (X + Y)\alpha_H)\,(2 + (X + Y)\alpha_P)}} \tag{A.12}$$

Due to the instability of the internal equilibrium host heterozygosity decays over time. Furthermore the larger the value of $\|\lambda\|$ the faster the heterozygosity should decay.

A.3.3. Simulations of a finite population

In analogy to the continuous-time model presented in the main-text where the death of the host and birth of the pathogen from infection are coupled, for our simulations in a finite population we assume $\alpha_H = \alpha_P = \alpha$. These Wright–Fisher simulations with fitnesses defined by Eq. (A.10) were run in *Mathematica* (see supplementary material). As with the continuous-time model we simulate coevolution for 50 random parameter sets of $X, Y,$ and, α ($0 < \alpha < 0.5,\ 0 < Y < X < 1$) and 7 values of κ (ranging on a log scale between 10^2 and $10^{3.5}$) for a total of 350 simulations. In contrast to the continuous-time model natural host death and free-living pathogen birth are incorporated directly in the Wright–Fisher model. For each of the simulations, sample paths were generated for 1000 independent replicate populations. All simulations are initialized at the internal polymorphic equilibrium and run for $t = 500$ generations.

In the absence of coevolution, the dynamics of host heterozygosity are given by the neutral expectation for the Wright–Fisher model:

$$H_{neut} = H_0 \left(1 - \frac{1}{\kappa}\right)^t \tag{A.13}$$

The difference between the simulated heterozygosity and the neutral expectation at time $t = 500$ is shown in Fig. A.1A. When population sizes is large ($\kappa = 3162$ upper right hand corner) the deviation in heterozygosity between the coevolutionary simulations and neutral expectation, $\Delta H = H_{coev} - H_{neut}$, is statistically negative as expected due to the erosion of genetic variation by coevolution. The magnitude of this deviation is however small, so while coevolution does indeed erode genetic variation the process is slow with only small effects over the parameter and time scale sampled.

As with the continuous-time model presented in the main text, directional selection (see Fig. A.1C) following fixation in the pathogen has a much larger effect than that of coevolutionary selection. When the population size is small (e.g. $\kappa = 100$), drift dominates over the effects of selection, and the heterozygosity behaves nearly neutrally. As the population size increases, the effect of this directional selection emerges. As predicted by the deterministic model variation in ΔH for a given population size is explained largely by variation in $\|\lambda\|$ (see Fig. A.1B). This is not only because $\|\lambda\|$ determines the effect of coevolution but because it is highly correlated with the probability of pathogen fixation and the strength of directional selection following pathogen fixation.

A.4. Seed dormancy

Here we extend the above discrete-time model to include the effects of seed dormancy, or any other process that causes

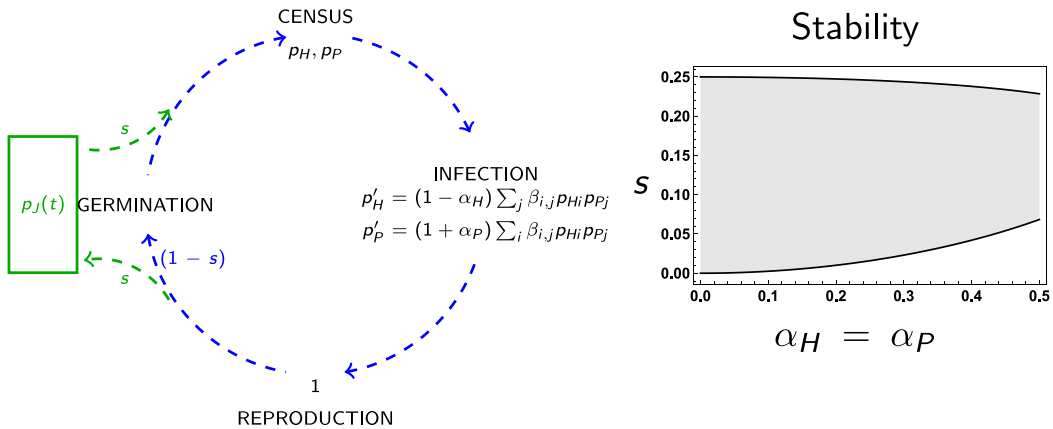

Fig. A.2. Life-cycle diagram and numerical stability analysis of the MAM with seed dormancy. Host and pathogen life-cycle (blue arrows), flux in and out of seed bank (green arrows). Shaded region of right-hand plot gives region for which the polymorphic equilibrium is stable assuming $\alpha_H = \alpha_P$ and given $X = 1, Y = 0$. (For interpretation of the references to colour in this figure legend, the reader is referred to the web version of this article.)

a subset, s, of the host population to avoid parasite induced selection, making the host less responsive during coevolution. Specifically, ever generation a proportion s of the reproducing host population is deposited into a seed bank and replaced by a germination of a random sample of seeds currently in the seed bank whereas a proportion $1-s$ of the reproducing host population produces seeds that immediately germinate. Seed can persist indefinitely once in the seed bank with the expected time to germination being geometrically distributed with probability p, creating a temporal asynchrony between host and parasite. We analyse the effect of this temporal asynchrony on the stability of the polymorphic equilibrium. Given a life cycle shown if Fig. A.2 we model evolution by following the allele frequencies among the host seedlings p_H, host juvenile seeds p_J, and within the parasite p_P. The dynamics are given by:

$$\begin{aligned} p_H(t+1) =& sp_J(t) + \frac{(1-s)p_H(t)(1-\alpha_H p_P(t)(X-Y)-\alpha_H Y)}{\alpha_H p_H(t)(1-2p_P(t))(X-Y)+\alpha_H p_P(t)(X-Y)-\alpha_H X+1} \\ p_J(t+1) =& (1-s)p_J(t) \\ &+ \frac{sp_H(t)(1-\alpha_H p_P(t)(X-Y)-\alpha_H Y)}{\alpha_H p_H(t)(1-2p_P(t))(X-Y)+\alpha_H p_P(t)(X-Y)-\alpha_H X+1} \\ p_P(t) =& \frac{p_P(t)(\alpha_P p_H(t)(X-Y)+\alpha_P Y+1)}{1-\alpha_P p_H(t)(1-2p_P(t))(X-Y)-\alpha_P p_P(t)(X-Y)+\alpha_P X} \end{aligned} \tag{A.14}$$

There are five equilibria of system (A.14), four of which are trivial fixation/loss of the host and pathogen. The fifth internal equilibrium is at $\hat{p}_H, \hat{p}_J, \hat{p}_P = \frac{1}{2}$. The Jacobian matrix at this internal equilibrium is given by:

$$J = \begin{bmatrix} 1-s & s & \frac{s(X-Y)\alpha_H}{\alpha_H(X+Y)-2} \\ s & 1-s & \frac{(1-s)(X-Y)\alpha_H}{\alpha_H(X+Y)-2} \\ 0 & \frac{s(X-Y)\alpha_P}{\alpha_P(X+Y)-2} & 1 \end{bmatrix} \tag{A.15}$$

Focusing on the diagonal elements, we note that $\frac{dp_H(t+1)}{dp_H(t)} < 1$ and $\frac{dp_J(t+1)}{dp_J(t)} < 1$. As noted by Tellier and Brown (2009) this is indicative of direct negative frequency-dependent selection. We can evaluate the stability of system (A.14) by using the Routh–Hurwitz conditions on the transformed characteristic polynomial of (A.15). Specifically, although the Routh–Hurwitz conditions can only be applied to identify the stability criteria in continuous time, if we transform the characteristic polynomial, $p(\lambda)$, into a third order polynomial in z such that:

$$(z-1)^3 p\left(\frac{z+1}{z-1}\right) = a_0 + a_1 z + a_2 z^2 + a_3 z^3 \tag{A.16}$$

then the equilibrium is stable (all eigenvalues have a magnitude less than 1) if and only if $a_i < 0\,\forall i$ and $a_2 a_1 - a_3 a_0 > 0$ assuming $\alpha_H = \alpha_P = \alpha$. These criteria are satisfied in our model for a range of s, indicating the internal equilibrium is stable under these conditions:

$$\begin{aligned} &\frac{\alpha^2(3X-Y)(X-3Y)+4-B}{\alpha^2 XY-1} < s < \frac{\alpha^2(3X-Y)(X-3Y)+4+B}{\alpha^2 XY-1} \\ &B = \sqrt{-(\alpha(X+Y)+2)(2-\alpha(X+Y))\left(\alpha^2\left(9X^2-14XY+9Y^2\right)-4\right)} \end{aligned} \tag{A.17}$$

where B must be real.

References

Agrawal, A., Lively, C.M., 2002. Infection genetics: Gene-for-gene versus matching-alleles models and all points in between. Evol. Ecol. Res. 4 (1), 79–90.

Ashby, B., Iritani, R., Best, A., White, A., Boots, M., 2019. Understanding the role of eco-evolutionary feedbacks in host-parasite coevolution. J. Theoret. Biol. 464, 115–125. http://dx.doi.org/10.1016/j.jtbi.2018.12.031.

Bodmer, W.F., 1972. Evolutionary significance of the HL-a system. Nature 237, 139–146.

Borghans, J., Beltman, J., De Boer, R., 2004. MHC polymorphism under host-pathogen coevolution. Immunogenetics.

Brown, J.K.M., Tellier, A., 2011. Plant-parasite coevolution: Bridging the gap between genetics and ecology. Annu. Rev. Phytopathol. 49 (1), 345–367. http://dx.doi.org/10.1146/annurev-phyto-072910-095301.

Chapman, J.R., Hill, T., Unckless, R.L., 2019. Balancing selection drives the maintenance of genetic variation in *Drosophila* antimicrobial peptides. Genome Biol. Evol. 11 (9), 2691–2701. http://dx.doi.org/10.1093/GBE/EVZ191.

Clarke, B., 1979. The evolution of genetic diversity. Proc. R. Soc. Lond. B 19–40.

Crow, J.F., 1970. Genetic loads and the cost of natural selection. In: Kojima, K.-i. (Ed.), Mathematical Topics in Population Genetics. In: Biomathematics, Springer, Berlin, Heidelberg, pp. 128–177.

Dybdahl, M.F., Jenkins, C.E., Nuismer, S.L., 2014. Identifying the molecular basis of host-parasite coevolution:Merging models and mechanisms. Am. Nat. 184 (1), 1–13. http://dx.doi.org/10.1086/676591.

Ejsmond, M., Radwan, J., 2015. Red queen processes drive positive selection on major histocompatibility complex (MHC) genes. PLoS Comput. Biol.

Flor, H., 1956. The complementary genic systems in flax and flax rust. Adv. Genet. 8, 29–54. http://dx.doi.org/10.1016/S0065-2660(08)60498-8.

Frank, S.A., 1991. Ecological and genetic models of host-pathogen coevolution. Heredity (September 1990), 73–83.

Frank, S.A., 1993. Specificity versus detectable polymorphism in host-parasite genetics. Proc. R. Soc. Lond. B 254 (1341), 191–197. http://dx.doi.org/10.1098/rspb.1993.0145.

Gandon, S., Capowiez, Y., Dubois, Y., Michalakis, Y., Olivieri, I., 1996. Local adaptation and gene-for-gene coevolution in a metapopulation model. Proc. R. Soc. Lond. B 263 (1373), 1003–1009. http://dx.doi.org/10.1098/rspb.1996.0148.

Gokhale, C., Papkou, A., Traulsen, A., Schulenburg, H., 2013. Lotka–Volterra dynamics kills the red queen: Population size fluctuations and associated stochasticity dramatically change host-parasite coevolution. BMC Evol. Biol. 13, http://dx.doi.org/10.1186/1471-2148-13-254, Artn 254.

Haldane, J., 1949. Disease and evolution. Ricerca Sci. Suppl. 19, 68–76.

Hamilton, W.D., 1993. Haploid dynamic polymorphism in a host with matching parasites: effects of mutation/subdivision, linkage, and patterns of selection. J. Hered. 84 (5), 328–338. http://dx.doi.org/10.1093/oxfordjournals.jhered.a111353.

Keeling, M.J., 2000. Metapopulation moments: Coupling, stochasticity and persistence. J. Animal Ecol. 69 (5), 725–736. http://dx.doi.org/10.1046/j.1365-2656.2000.00430.x.

Klein, J., 1987. Origin of major histocompatibility complex polymorphism: The trans-species hypothesis. Human Immunol. 19 (3), 155–162. http://dx.doi.org/10.1016/0198-8859(87)90066-8.

Klein, J., Figueroa, F., 1986. Evolution of the major histocompatibility complex. Crit. Rev. Immunol. 6 (4), 295–386.

Lawlor, D.A., Ward, F.E., Ennis, P.D., Jackson, A.P., Parham, P., 1988. HLA-a and b polymorphisms predate the divergence of humans and chimpanzees. Nature 335 (6187), 268–271. http://dx.doi.org/10.1038/335268a0.

Lively, C.M., 1999. Migration, virulence, and the geographic mosaic of adaptation by parasites. Am. Nat. 153 (Suppl.), 34–47. http://dx.doi.org/10.1086/303210.

Llaurens, V., Whibley, A., Joron, M., 2017. Genetic architecture and balancing selection: The life and death of differentiated variants. Mol. Ecol. 26 (9), 2430–2448. http://dx.doi.org/10.1111/mec.14051.

MacPherson, A., Keeling, M.J., Otto, S.P., 2020. Feedback between coevolution and epidemiology can help or hinder the maintenance of genetic variation in host-parasite models. http://dx.doi.org/10.1101/2020.04.07.029322, bioRxiv, 2020.04.07.029322.

MacPherson, A., Otto, S.P., 2018. Joint coevolutionary– epidemiological models dampen Red Queen cycles and alter conditions for epidemics. Theor. Popul. Biol. 122, 137–148. http://dx.doi.org/10.1016/j.tpb.2017.12.003.

McConnell, T.J., Talbot, W.S., McIndoe, R.A., Wakeland, E.K., 1988. The origin of MHC class II gene polymorphism within the genus mus. Nature 332 (6165), 651–654. http://dx.doi.org/10.1038/332651a0.

M'Gonigle, L.K., Otto, S.P., 2011. Ploidy and the evolution of parasitism. Proc. R. Soc. Lond. B 278 (1719), 2814–2822. http://dx.doi.org/10.1098/rspb.2010.2146.

M'Gonigle, L.K., Shen, J.J., Otto, S.P., 2009. Mutating away from your enemies: The evolution of mutation rate in a host-parasite system. Theor. Popul. Biol. 75 (4), 301–311. http://dx.doi.org/10.1016/j.tpb.2009.03.003.

Moran, P.A.P., 1958. Random processes in genetics. Math. Proc. Camb. Phil. Soc. 54 (1), 60–71. http://dx.doi.org/10.1017/S0305004100033193.

Nuismer, S.L., 2006. Parasite local adaptation in a geographic mosaic. Evolution 60 (1), 24. http://dx.doi.org/10.1554/05-380.1.

Nuismer, S.L., 2017. Introduction to Coevolutionary Theory, first ed. Macmillan Learning, New York.

Nuismer, S.L., Otto, S.P., 2004. Host-parasite interactions and the evolution of ploidy. Proc. Natl. Acad. Sci. USA 101 (30), 11036–11039. http://dx.doi.org/10.1073/pnas.0403151101.

Otto, S.P., Michalakis, Y., 1998. The evolution of recombination in changing environments. Nat. Rev. Genet. 13 (4), 145–151.

Papkou, A., Gokhale, C.S., Traulsen, A., Schulenburg, H., 2016. Host– parasite coevolution: Why changing population size matters. Zoology 119 (4), 330–338. http://dx.doi.org/10.1016/j.zool.2016.02.001.

Rabajante, J.F., Tubay, J.M., Ito, H., Uehara, T., Kakishima, S., Morita, S., Yoshimura, J., Ebert, D., 2016. Host-parasite Red Queen dynamics with phase-locked rare genotypes. Sci. Adv. 2 (3), e1501548. http://dx.doi.org/10.1126/sciadv.1501548.

Sasaki, A., 2000. Host-parasite coevolution in a multilocus gene-for-gene system. Proc. R. Soc. Lond. B 267 (1458), 2183–2188. http://dx.doi.org/10.1098/rspb.2000.1267.

Schenk, H., Schulenburg, H., Traulsen, A., 2018. Suicidal Red Queen: Population dynamics and genetic drift accelerate diversity loss. 490201. http://dx.doi.org/10.1101/490201, bioRxiv.

Schenk, H., Schulenburg, H., Traulsen, A., 2020. How long do Red Queen dynamics survive under genetic drift? A comparative analysis of evolutionary and eco-evolutionary models. BMC Evol. Biol. 20 (1), 8. http://dx.doi.org/10.1186/s12862-019-1562-5.

Segar, J., Hamilton, W.D., 1988. Parasites and Sex. In: The Evolution of Sex: An Examination of Current Ideas. Sinauer Associates, The University of Michigan, pp. 176–193.

Takahata, N., Nei, M., 1990. Allelic genealogy under overdominant and frequency-dependent selection and polymorphism of major histocompatibility complex loci. Genetics (124), 967–978.

Tellier, A., Brown, J.K., 2009. The influence of perenniality and seed banks on polymorphism in plant-parasite interactions. Am. Nat. 174 (6), 769–779. http://dx.doi.org/10.1086/646603.

Tellier, A., Moreno-Gámez, S., Stephan, W., 2014. Speed of adaptation and genomic footprints of host-parasite coevolution under arms race and trench warfare dynamics. Evolution 68 (8), 2211–2224. http://dx.doi.org/10.1111/evo.12427.

Unckless, R.L., Lazzaro, B.P., Unckless, R.L., 2016. The potential for adaptive maintenance of diversity in insect antimicrobial peptides. Philos. Trans. R. Soc. B.

Veller, C., Hayward, L.K., Hilbe, C., Nowak, M.A., 2017. The Red Queen and King in finite populations. Proc. Natl. Acad. Sci. 114 (27), E5396–E5405. http://dx.doi.org/10.1073/pnas.1702020114.

Wakeley, J., 2016. Coalescent Theory: An Introduction. Macmillan Learning, Google-Books-ID: x30RAgAACAAJ.

Woolhouse, M.E.J., Webster, J.P., Domingo, E., Charlesworth, B., Levin, B.R., 2002. Biological and biomedical implications of the co-evolution of pathogens and their hosts. Nature Genet. 32 (4), 569–577. http://dx.doi.org/10.1038/ng1202-569.

Xue, C., Goldenfeld, N., 2017. Coevolution maintains diversity in the stochastic "Kill the Winner" model. Phys. Rev. Lett. 119 (26), 268101. http://dx.doi.org/10.1103/PhysRevLett.119.268101.

Ye, T.Z., Yang, R.-C., Yeh, F.C., 2003. Coevolution in natural pathosystems: Effects of dominance on host-pathogen interactions. Phytopathology 93 (5), 633–639. http://dx.doi.org/10.1094/PHYTO.2003.93.5.633.

Zhao, L., Waxman, D., 2016. The influence of genetic drift on the formation and stability of polymorphisms arising from negative frequency-dependent selection. J. Theoret. Biol. 391, 51–64. http://dx.doi.org/10.1016/j.jtbi.2015.11.011.

Zimmer, C., Emlen, D.J., 2013. Evolution: Making Sense of Life, second ed. W.H. Freeman & Company.